

STERNHEIMERGW: a program for calculating GW quasiparticle band structures and spectral functions without unoccupied states

Martin Schlipf*, Henry Lambert¹, Nourdine Zibouche, Feliciano Giustino*

Department of Materials, University of Oxford, Parks Road, Oxford OX1 3PH, United Kingdom

Abstract

The STERNHEIMERGW software uses time-dependent density-functional perturbation theory to evaluate GW quasiparticle band structures and spectral functions for solids. Both the Green's function G and the screened Coulomb interaction W are obtained by solving linear Sternheimer equations, thus overcoming the need for a summation over unoccupied states. The code targets the calculation of accurate spectral properties by convoluting G and W using a full frequency integration. The linear response approach allows users to evaluate the spectral function at arbitrary electron wavevectors, which is particularly useful for indirect band gap semiconductors and for simulations of angle-resolved photoelectron spectra. The software is parallelized efficiently, integrates with version 6.3 of Quantum Espresso, and is continuously monitored for stability using a test farm.

Keywords: first-principles calculations, many-body perturbation theory, solid state physics, linear response

Program Summary

Program Title: STERNHEIMERGW

Licensing provisions: GNU General Public License v3.0

Programming language: Fortran 2003

Nature of problem: The lack of the exchange-correlation discontinuity in density-functional theory (DFT) leads to a systematic underestimation of the band gap between conduction and valence states. Many-body perturbation theory in the GW approximation provides an effective solution to this problem, as well as other limitations faced by DFT in the description of electronic excitations. However, the GW method comes with its own set of limitations: (i) The perturbation of the system is typically expressed in terms of the unoccupied states, and achieving numerical convergence with respect to these states is often cumbersome. Since the underlying DFT codes rely only on the occupied states, their default behavior is often ill-suited to provide a sufficient amount of empty states. Combined with the large number of parameters that need to be converged, this limits the use of GW codes by non-expert users and automatic scripts. (ii) Currently, GW codes require that a homogeneous k -point

mesh is used in the calculation. Hence, features close to the band edges are often only accessible via prohibitively expensive dense k -point meshes or interpolation techniques. (iii) To evaluate the frequency convolution of the Green's function G and the screened Coulomb interaction W , many current GW calculations rely on approximations such as the plasmon-pole approximation, the analytic continuation, or the contour deformation. The relative merits and accuracy of the various approximations are not fully understood.

Solution method: In STERNHEIMERGW, we address (i) by replacing the summation over unoccupied states with a linear response equation. The solution depends on the occupied states only, and it employs linear response algorithms already provided by the Quantum ESPRESSO suite to compute phonons and related properties. As an additional benefit, transforming the problem in a linear response equation removes the restriction to homogeneous k -point meshes (ii), so that the GW self-energy for any arbitrary point can be evaluated. Finally (iii), we provide the possibility to perform a full frequency convolution along the real frequency axis. This feature can serve as a benchmark for approximate integrations using models or analytic continuation.

*Corresponding authors.

E-mail addresses: martin.schlipf@gmail.com (M. Schlipf), feliciano.giustino@materials.ox.ac.uk (F. Giustino).

¹Present address: Kings College London, Physics Department, Strand, London WC2R 2LS, United Kingdom.

1. Introduction

Kohn-Sham density function theory (DFT)³⁻⁵ is a powerful and extremely popular formalism for studying the total energy of an interacting electron system in its ground state. When used in the study of electronic excitations, such as the calculation of electron band structures and wavefunctions, DFT exhibits some well known deficiencies, for example the lack of the exchange-correlation discontinuity in the exchange-correlation potential,^{6,7} which leads to an underestimation of the band gap in insulators, and the excessive delocalization of *d* and *f* electrons. Applying many-body perturbation theory corrections in the *GW* approximation^{8,9} allows one to correct some of these deficiencies using the non-local and frequency-dependent electron self-energy $\Sigma(\omega)$. Early numerical implementations of this method demonstrated an improved band gap for diamond^{10,11} and similar improvement were subsequently shown for other typical semiconductors.^{12,13} Since then, *GW* has been used to accurately describe the band gaps for a variety of systems ranging from solids to interfaces and molecules.¹⁴⁻¹⁷ It yields accurate band offsets¹⁸, defect energies,¹⁹ and improved effective masses.²⁰ Recent developments focused on the self-consistency of the *GW* method for molecules²¹⁻²³ and solids,²⁴ as well as total energy calculations.^{25,26}

More recent developments of the *GW* method relate to photoelectron spectroscopy. Progress in high-energy

resolution angle-resolved photoelectron spectroscopy (ARPES) had led to a renewed interest in the spectral function of materials, in particular the signatures of electron correlations and bosonic excitations. These features were originally examined for the homogeneous electron gas,^{9,27-30} but have recently been investigated both experimentally and theoretically for charge carriers in semiconductors coupling to plasmons,^{1,31-43} Fröhlich polarons⁴⁴⁻⁵⁵ or hybridizations of these excitations.^{56,57} While the *GW* approximation does produce satellite features in the spectral function, their strength is overestimated and their energy is blue-shifted.^{27-29,32,58} This mismatch is intrinsic to the *GW* approximation and cannot be overcome by self-consistency.^{23,41,59,60} Nevertheless, the *GW* spectral function can provide a starting point for the cumulant expansion, in which the satellite and quasiparticle spectral function are convoluted and the position and weight of the satellite features are corrected.^{14,54,61-67}

At present, there are two major limitations to obtain accurate spectral functions with the *GW* approximation. First, the frequency dependence of the screened Coulomb interaction is commonly approximated by a Dirac delta function in the plasmon-pole model.^{12,68,69} To increase the accuracy, more recent approaches employ an analytic continuation⁷⁰⁻⁷² or contour deformation.⁷³⁻⁷⁵ A detailed assessment of the accuracy of these techniques is still lacking and may prove crucial for re-

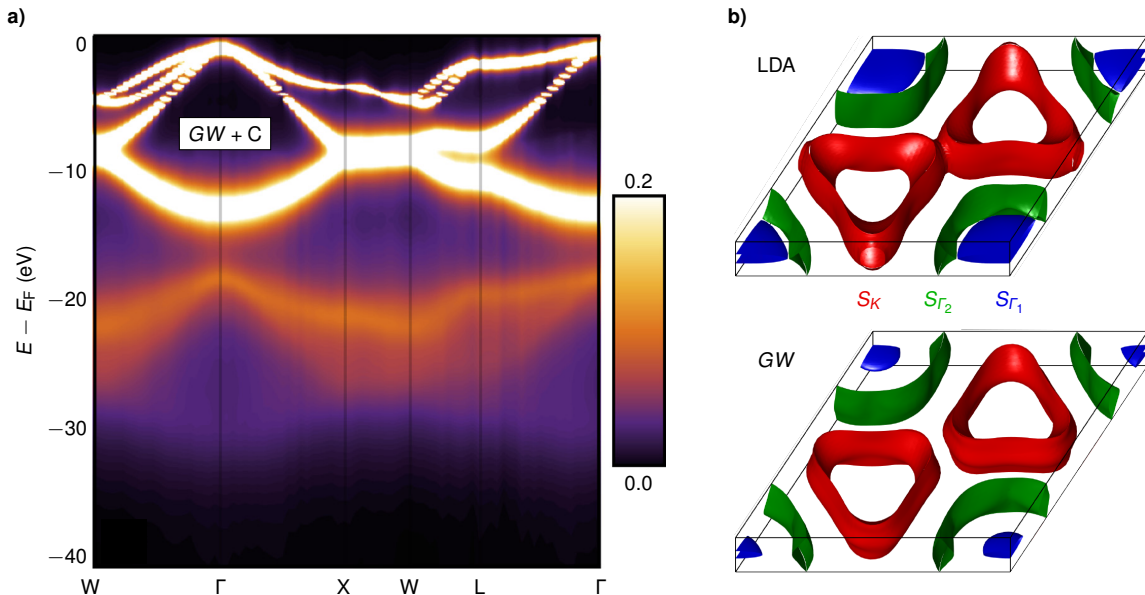


Figure 1: Examples of recent calculations performed with the STERNHEIMERGW code. **a)** Spectral function of silicon (eV^{-1}) using the *GW* + cumulant expansion approach. Reproduced with permission from Ref. 1. **b)** Comparison of the LDA and *GW* Fermi surfaces of bulk NbS_2 near the Γ (blue and green) and the K point (red). Reproduced with permission from Ref. 2.

liable calculations of quasiparticle lifetimes.^{76,77} Secondly, most *GW* implementations rely on a summation over the empty Kohn-Sham states.¹² This requires a very accurate description of the unoccupied subspace and therefore imposes additional constraints on the construction of pseudopotentials. Furthermore, converging the eigenvalues occasionally demands the inclusion of a considerable number of empty states^{78–80}, and the convergence with respect to these states is interdependent with other convergence parameters.^{79,81} To address these issues, several techniques have been proposed^{82–87} which improve the rate of convergence of the summations. However, some of these methods introduce additional convergence parameters. Alternatively, one can obtain the dielectric matrix in density-functional perturbation theory^{88,89} by solving linear Sternheimer equations.⁹⁰ This approach has been subsequently optimized by iterative diagonalization to determine the most significant eigenvalues^{91–93} or employing an optimal representation of the polarization.^{94,95} One can extend this approach, so that both the Green’s function G and the screened Coulomb interaction W can be obtained by solving linear response equations.^{94,96} This approach is referred to as the *Sternheimer GW* method and has been successfully applied to large systems with a single \mathbf{k} point.^{94,95,97}

In this work, we develop an implementation for solids building on the methodology described in Ref. 96 and 98. Our implementation, called STERNHEIMERGW, features the plasmon pole model, the analytic continuation, as well as the real frequency integration on the same footing, and is therefore suitable to assess the accuracy of these techniques. The frequency dependent self-energy allows us to access spectral properties from first principles.⁷⁷ Two illustrative examples of the application of STERNHEIMERGW are shown in Fig. 1. In Fig. 1a we show the complete wavevector-dependent spectral function of silicon. For these results the frequency-dependent self-energy obtained with STERNHEIMERGW is used as a starting point for a cumulant expansion, to obtain both quasiparticle band structure and plasmon replicas with the correct energy and intensity.^{1,40} In Fig. 1b, we show the use of STERNHEIMERGW to evaluate the Fermi surface of the transition metal dichalcogenide NbS₂.² In this system, the change of density of states at the Fermi energy due to many-body perturbation theory corrections is important to obtain more accurate predictions for the superconducting transition temperature.⁹⁹

2. Description of the code

2.1. Kohn-Sham reference system

To evaluate the many-body perturbation correction, we start from an unperturbed reference system within Kohn-Sham density functional theory. The important ingredients of this reference system for our calculation are the exchange-correlation potential V^{xc} and the Kohn-Sham Hamiltonian $\hat{H}_{\mathbf{k}}$ along with its eigenvalues $\varepsilon_{n\mathbf{k}}$ and wavefunctions $\phi_{n\mathbf{k}}(\mathbf{r})$. Here n is a band index, \mathbf{r} is the position vector, and \mathbf{k} a Bloch vector in the Brillouin zone of the crystal. We employ a planewaves basis set, and express the wavefunction $\phi_{n\mathbf{k}}(\mathbf{r})$ in terms of the expansion coefficients $u_{n\mathbf{k},\mathbf{G}}$:

$$\phi_{n\mathbf{k}}(\mathbf{r}) = \frac{1}{\sqrt{\Omega}} \sum_{\mathbf{G}} u_{n\mathbf{k},\mathbf{G}} \exp[i(\mathbf{k} + \mathbf{G}) \cdot \mathbf{r}], \quad (1)$$

where \mathbf{G} denotes reciprocal lattice vectors and Ω is the volume of the unit cell. In a planewaves basis only the kinetic energy part of the Hamiltonian and the non-local part of the pseudopotentials are represented in reciprocal space; the local Kohn-Sham potential is applied in real space via a fast Fourier transform.

2.2. Green’s function

From the Kohn-Sham Hamiltonian, we obtain the electronic Green’s function, which is one of the ingredients to evaluate the *GW* self-energy. The Green’s function is given by the linear equation:

$$\forall_{\mathbf{k},\mathbf{G}'} \quad \mathcal{L}_{\mathbf{k}}^{\mathbf{G}}(\omega) G_{\mathbf{G}\mathbf{G}'}(\omega) = -\delta_{\mathbf{G}\mathbf{G}'}. \quad (2)$$

Here, ω is a complex frequency, chosen to satisfy the time ordering, $\mathcal{L}^{\mathbf{G}}$ is the linear operator for the Green’s function:

$$\mathcal{L}_{\mathbf{k}}^{\mathbf{G}}(\omega) = \hat{H}_{\mathbf{k}} - \hbar\omega, \quad (3)$$

and $\delta_{\mathbf{G}\mathbf{G}'}$ is the Kronecker δ . Most *GW* codes expand Eq. (2) in the basis of the eigenstates of the Hamiltonian and solve it by summing over many unoccupied states. In contrast, in STERNHEIMERGW we utilize an iterative Krylov subspace solver¹⁰⁰ to explicitly find the solution to the linear equation (2). We employ the fact that shifted linear problems described by the linear operator $\mathcal{L}^{\mathbf{G}}$ differing only in the frequency ω span the same Krylov subspace. This property allows us to solve the linear problem for all frequencies at the computational complexity of a single frequency.

2.3. Dielectric matrix

The dielectric matrix of a system can be evaluated from the electron density response to a planewave perturbation:

$$\epsilon_{q,GG'}(\omega) = \delta_{GG'} - \Delta n_{q,GG'}(\omega), \quad (4)$$

where ω is the frequency. The calculation of the density response is performed by starting from the linear variation of the wavefunctions in real space, and then carrying out a Fourier transform into reciprocal space:

$$\Delta n_{q,rG'}(\omega) = 2 \frac{1}{N_k} \sum_{nk,\pm}^{\text{occ.}} u_{nk,r}^* \Delta u_{nk+q,rG'}(\pm\omega), \quad (5)$$

where the factor 2 accounts for the spin degeneracy and we are assuming a uniform grid of N_k \mathbf{k} -vectors in the Brillouin zone. The change of the wavefunction coefficients is obtained from the Sternheimer equation, which can be written as:

$$\forall_{nk,G} \quad \mathcal{L}_{k+q}^C \left(\frac{\epsilon_{nk+q}}{\hbar} + \omega \right) \Delta u_{nk+q,GG'}(\omega) = \delta u_{nk,GG'}. \quad (6)$$

Since the linear operator of the Coulomb response,

$$\mathcal{L}_k^C(\omega) = \hat{H}_k - \hbar\omega + \hat{P}^{\text{occ}}, \quad (7)$$

is very similar to the one for the Green's function (3), the same Krylov subspace solvers can be employed. The only difference with respect to (3) is that now we have an additional projector on the occupied states \hat{P}^{occ} ; this term improves the condition number of the linear operator. The right-hand side of (6) is given by a Fourier transform of:

$$\delta u_{nk,G'r'} = (1 - \hat{P}^{\text{occ}}) e^{iG'r'} u_{nk,r'}, \quad (8)$$

and describes a driving field corresponding to a periodic perturbation.

2.4. Correlation self-energy

For the correlation self-energy, we combine the inverse of the dielectric matrix with the truncated Coulomb potential (see Sec. 2.6):

$$\bar{W}_{q,GG'}(\omega) = v_{q+G} (\epsilon_{q,GG'}^{-1}(\omega) - \delta_{GG'}), \quad (9)$$

where \bar{W} is the correlation part of the screened Coulomb interaction. To overcome numerical issues associated with the inversion of the dielectric matrix for $q \approx 0$,¹⁰¹ we evaluate that element for a small but finite q ¹⁰² and set the off-diagonal elements to zero if $\mathbf{q} + \mathbf{G} = \mathbf{0}$ or

$\mathbf{q} + \mathbf{G}' = \mathbf{0}$.¹⁰³ Subsequently, we perform a Fourier transform of G and \bar{W} to real space, because the self-energy can be expressed as a product there:

$$\Sigma_{k,rr'}^c(\omega) = \sum_{\omega'q} \frac{\alpha w_{\omega'} w_q}{2\pi} G_{k-q,rr'}(\omega') \bar{W}_{q,rr'}(\omega' - \omega). \quad (10)$$

w_q and $w_{\omega'}$ are weights for \mathbf{q} and ω integration respectively. The factor α depends on whether the frequency integration is performed along the real axis ($\alpha = i$) or along the imaginary axis ($\alpha = -1$). We transform the resulting self-energy back to reciprocal space to evaluate the expectation values with the Kohn-Sham wavefunctions.

2.5. Exchange self-energy

To evaluate the exchange self-energy, we evaluate the Fock potential by summing over all occupied wavefunctions:

$$\Sigma_{k,GG'}^x = - \sum_{nq,G''}^{\text{occ.}} \frac{w_{nk-q}}{\Omega} u_{nk-q,G''}^* u_{nk-q,G-G''} v_{q+G''}, \quad (11)$$

where the weight w_{nk-q} contains the weight of the \mathbf{q} integration. The Coulomb potential is truncated as described in the following section.

2.6. Truncation

Owing to the long-range nature of the Coulomb potential, the Fourier transform of this quantity diverges for small arguments $q \rightarrow 0$, leading to instabilities in the convergence with respect to the grid in the Brillouin zone. Furthermore, when describing systems of reduced dimensionality, such as slabs or nanowires, it is advantageous to truncate the Coulomb potential along the non-periodic direction in order to avoid spurious interactions between periodic images. In order to address these issues, it is common practice to truncate¹⁰⁴⁻¹⁰⁶ the Coulomb potential at a certain distance. This approach yields a Fourier transform with a finite value in the limit $q \rightarrow 0$. In STERNHEIMERGW, we implement three different truncation schemes: First, one can truncate the Coulomb potential at a distance R_{cut} (*spherical truncation*) resulting in a potential:

$$v_q = \frac{e^2}{4\pi\epsilon_0} \frac{4\pi}{q^2} [1 - \cos(qR_{\text{cut}})]. \quad (12)$$

Secondly, one can truncate the Coulomb interaction at a height z_{cut} (*slab truncation*), which yields the following potential:¹⁰⁴

$$v_q = \frac{e^2}{4\pi\epsilon_0} \frac{4\pi}{q^2} \left[1 - \exp(-\sqrt{q_x^2 + q_y^2} z_{\text{cut}}) \right] \cos(q_z z_{\text{cut}}). \quad (13)$$

Lastly, one can truncate the Coulomb interaction in the Wigner-Seitz supercell.¹⁰⁶ In this latter case, since an analytic expression for the potential is not known, we tabulate the results of the truncation and look up the values for the relevant vectors as necessary.

2.7. Analytic continuation

Quantities such as the dielectric matrix and the self-energy exhibit significant structure along the real axis, for example due to electron-hole excitations. In order to improve numerical stability and accuracy, it can be advantageous to evaluate quantities along the imaginary axis and perform an analytic continuation to the real axis. In STERNHEIMERGW, there are two levels where such an analytic continuation may be employed. On the one hand, one can evaluate the dielectric function on the imaginary axis, perform an analytic continuation to the real axis, and subsequently convolute it with the Green's function according to Eq. (10). On the other hand, one can resolve the convolution along the imaginary axis, thereby obtaining a self-energy at imaginary frequency values. The self-energy at real frequencies is then obtained via analytic continuation. To perform the analytic continuation, one can use a Padé expansion¹⁰⁷ or the adaptive Antoulas-Anderson (AAA) algorithm.¹⁰⁸ In general, determining the Padé approximant using a continued fraction expansion suffers from numerical instabilities, since a very high precision (number of significant digits) is required. In contrast, the AAA algorithm relies on a singular-value decomposition, and it refines iteratively the data points used to construct the approx-

imant, until the largest deviation falls below a specified threshold.

2.8. Spectral function

The spectral function is related to the imaginary part of the retarded Green's function:

$$A_{k,GG'}(\omega) = -\frac{1}{\pi} \text{Im}(G_{k,GG'}(\omega)), \quad (14)$$

and represents a \mathbf{k} -resolved many-body density of states. Since the Green's function is the resolvent of the many-body Hamiltonian, this leads to:

$$A_{k,GG'}(\omega) = -\frac{1}{\pi} \text{Im}(\hbar\omega - H_k - \Sigma_k^{\text{xc}}(\omega) + V_k^{\text{xc}})_{GG'}^{-1}. \quad (15)$$

Approximating the GW wavefunctions by their Kohn-Sham counterpart $\phi_{nk}(\mathbf{r})$, the diagonal part of the spectral function in the Kohn-Sham basis can be expressed as:

$$A_{nk}(\omega) = \frac{-\text{Im}\Sigma_{nk}^c(\omega)}{\pi \left| \hbar\omega - \varepsilon_{nk} - \text{Re}\Sigma_{nk}^c(\omega) + V_{nk}^{\text{xc}} \right|^2}. \quad (16)$$

The peaks of the spectral function correspond to the quasiparticle eigenvalues. Linearizing the equation in the vicinity of the eigenvalue ε_{nk} results in the following quasiparticle eigenvalue:

$$\varepsilon_{nk}^{\text{QP}} = \varepsilon_{nk} + Z_{nk} \left(\text{Re}\Sigma_{nk}^c(\varepsilon_{nk}/\hbar) - V_{nk}^{\text{xc}} \right), \quad (17)$$

where $Z_{nk} = 1 - \hbar^{-1} \text{Re}(\partial\Sigma_{nk}^c/\partial\omega)$.

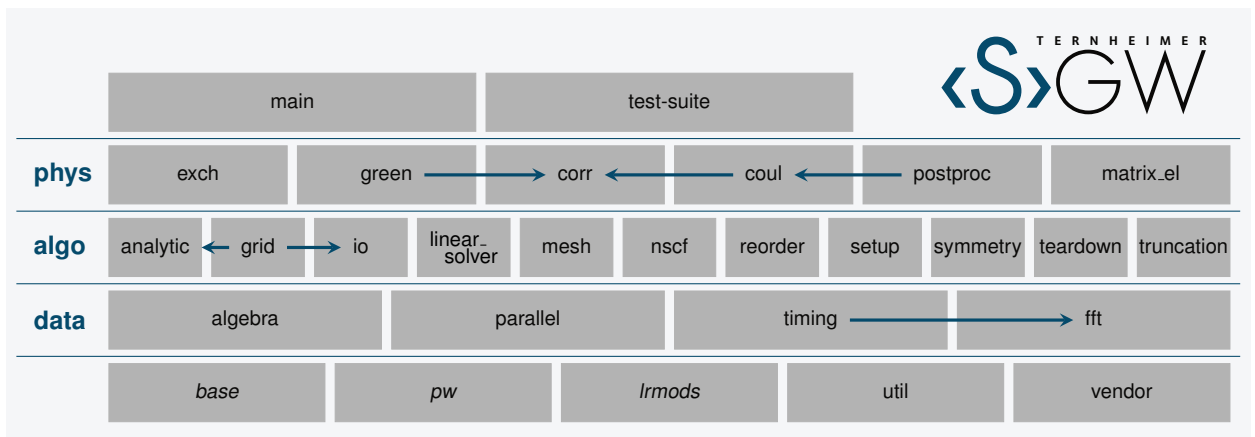


Figure 2: Multitier architecture of the STERNHEIMERGW code. The lowest tier includes external libraries as well as a utility package. The packages written in italic are not distributed with the STERNHEIMERGW code and require the Quantum ESPRESSO software. In the *data* tier, we implement wrappers to these libraries. We combine these packages in the *algo* tier to provide the necessary data structures and algorithms, which are used in the *phys* tier to solve the physical problem. The highest tier interacts with the user and is used for testing the program. Arrows indicate dependencies within the same tier.

2.9. Software design

Architecture. In Fig. 2, we illustrate the multitier architecture of STERNHEIMERGW. The code builds on functionality provided by the Quantum Espresso software package^{109,110} and provides additional functionality handling low-level operations in the *data* tier. On top of this layer, we have an *algo* tier handling the interface with Quantum Espresso. The *algo* tier also provides integration grids, linear solvers, Coulomb truncation, and analytic continuation functionalities. In the *phys* tier, we evaluate the *GW* self-energy and matrix elements, employing the functionality of the lower lying tiers. The highest tier provides the user interface and the infrastructure for testing the software.

User input. The typical approach for specifying the user interface of a code requires that changes to input variables are manually translated into an update of the documentation. As this scheme poses the risk that the documentation becomes outdated, we employ an inverse scheme in STERNHEIMERGW. The core file controlling the user input is a human- and machine-readable YAML file documenting all input variables (see example in Fig. 3a). Starting from the documentation, we run a script to generate the Fortran file that processes the input file (Fig. 3b). As a consequence, introducing a new input variable requires an update of the documentation. This strategy allows us to make sure that the code

Table 1: Combined code coverage of integration and unit tests, i.e., the fraction of F90 lines and subroutines of the code that are executed at least once by the test set. The higher tiers are covered exclusively by the integration tests; for the lower tiers unit tests play a large role.

	main	phys	algo	data
<i>F90 lines</i>				
integration tests	100.0%	92.1%	70.3%	31.4%
unit tests	0.0%	0.0%	41.3%	74.3%
combined	100.0%	92.1%	86.7%	92.3%
<i>subroutines</i>				
integration tests	100.0%	97.3%	64.6%	30.0%
unit tests	0.0%	0.0%	53.3%	80.0%
combined	100.0%	97.3%	87.7%	93.3%

and the documentation are always in sync. Furthermore, we process the YAML file to generate the online documentation of STERNHEIMERGW (Fig. 3c) on the website <http://sternheimergw.org>.

Continuous integration and testing. To ensure the long-term stability of the code and its alignment with the Quantum Espresso suite, we employ two techniques. First, we examine whether the code compiles and reproduces a set of reference results using a buildbot test farm.^{111,112} These integration tests involve 12 different calculations to check most of the functionality of STERNHEIMERGW. Secondly, we perform unit testing of some individual packages of the code, by benchmarking

a)

```
gw_input:
  num_band:
    type: integer
    default: 0
    description: Number of bands for which the GW correction is evaluated. Note that it has to
      be larger than the number of occupied states so that the Fermi energy can be calculated.
```

b)

```
MODULE gw_input_module

  TYPE gw_input_type
    INTEGER :: num_band = 0
  END TYPE gw_input_type

CONTAINS

  ! logic to read input file, broadcast the
  ! results and store them in a gw_input_type

END MODULE gw_input_module
```

c)

Figure 3: Automatic generation of the user-input logic in SternheimerGW: **a)** The `gw_input.yml` file defines which input variables are used in STERNHEIMERGW along with their type, default value, and a description. **b)** A script processes the YAML file to generate a Fortran file containing a type with all input variables and the logic to read them. **c)** The YAML file is also processed to generate the description of the input variables on the website <http://sternheimergw.org>.

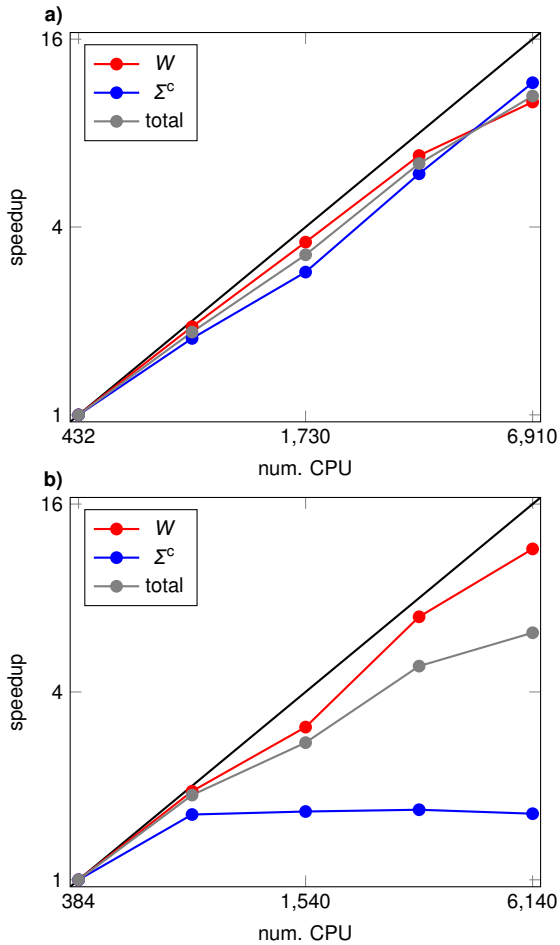


Figure 4: Parallel efficiency of the STERNHEIMERGW code for the screened Coulomb interaction W (red), the correlation self-energy Σ^c (blue), and the whole code (gray) using a) pool parallelization and b) image parallelization. Measured for a bulk calculation of MgO on MareNostrum 4, BSC-CNS (Spain) with converged parameters as listed in Table 3.

the parallelization, the algebra, the analytic continuation, the linear solver, and the input/output (io) package independently from the rest of the code. For the unit testing, at variance with the tests of the complete code, we compare our implementation with analytic results. The unit tests are implemented in the pFUnit framework.¹¹³ Overall, all these tests cover at least 80% of the code in each tier (see Table 1).

2.10. Parallelization

GW calculations are computationally much more demanding than Kohn-Sham DFT calculations. To allow for a reasonable time to solution, we employ two different parallelization levels in STERNHEIMERGW. As we inherit the distribution logic from Quantum Espresso,

Table 2: Comparison of the band gap of a selected set of materials with reference results from the literature. All values are given in eV. Numerical parameters used for the calculations are listed in Table 3.

	Present	Ref. 114	Ref. 115	Ref. 116	Ref. 117
BN	6.27	6.10	6.20		6.19
C	5.53	5.50	5.62	5.62	5.59
CdS	2.20	2.06	2.18		2.31
GaAs	1.23	1.30	1.31	1.21	1.10
Ge	0.78		0.75	0.63	0.50
MgO	7.13	7.25	7.17	6.71	7.08
Si	1.17	1.12	1.11	1.26	1.17

we refer to these levels as *pool* and *image* parallelization. In Fig. 4, we compare the performance of these parallelization levels for a bulk system of MgO for different parts of the code. With the pool parallelization, we distribute different k or q points to different processors. This method is very efficient for both G and W , if the number of these points is a multiple of the number of CPUs. The image parallelization distributes G vectors used in the linear response and Fourier transform to different CPU. For the calculation of W , this parallelization is very efficient because the solution of the linear-response equation for each G vector is independent of the other G vectors. When evaluating Σ^c the speedup of this parallelization saturates when the number of grid points along the z axis reduces to one per CPU. The benefit of the image parallelization is that it reduces the memory footprint of the code.

3. Examples

3.1. Benchmark results

To assess the accuracy of STERNHEIMERGW, we verify the implementation by comparing to reference calculations from the literature.^{114–117} We use seven reference systems in the diamond (C, Si, and Ge), the zincblende (BN, CdS, and GaAs), or rocksalt structure (MgO). All lattice constants are taken from Ref. 114, except for that of Ge which is from Ref. 120.

The DFT ground state calculation was run with Quantum ESPRESSO v6.3 using a $12 \times 12 \times 12$ k -point mesh and the PBE exchange-correlation potential.¹²¹ The pseudopotentials are verified according to the Δ -test;¹²² as a compromise between speed and accuracy, we employ the ONCV¹²³ pseudopotentials from the SG15 library¹¹⁸ for compounds not including d electrons, and the stringent pseudopotentials v0.4 from pseudo-dojo.org¹¹⁹ otherwise.

In Table 2, we present the comparison between the reference calculations and the results obtained with

Table 3: Convergence parameters used in the calculation of the GW corrections reported in Table 2: The pseudopotentials (PP) are from the SG15 library¹¹⁸ or the stringent ones from `pseudo-dojo.org`;¹¹⁹ the energy cutoffs are employed for the DFT self-consistent field cycle (scf), the exchange (x) or the correlation (c) self energy; the integration grids for the self-energy and the density response are homogeneous grids with N_q and N_k points; the coarse frequency mesh for W are obtained from a $(N_\omega - 1)$ -node Gauss-Laguerre quadrature along the imaginary axis including the origin, and extending up to $\hbar\hat{\omega}$; and the dense mesh for W as well as the coarse one for Σ are automatically constructed by the code. The row with the dagger contains the loose values used for the convergence test and the row with the asterisk is used for the convolution along the real frequency axis.

material	PP	energy cutoffs (Ry)					coarse, W		dense, W		coarse, Σ		threshold	
		$E_{\text{cut}}^{\text{scf}}$	E_{cut}^x	E_{cut}^c	$N_q^{1/3}$	$N_k^{1/3}$	N_ω	$\hbar\hat{\omega}$ (eV)	N_ω	$\hbar\hat{\omega}$ (eV)	N_ω	$\hbar\hat{\omega}$ (eV)	t_W	t_G
BN	SG15	60	50	40	8	8	31	104	80	320	20	150	10^{-4}	10^{-5}
C	SG15	70	50	24	8	8	31	104	50	280	30	180	10^{-4}	10^{-5}
CdS	Dojo	60	55	25	8	8	31	104	150	150	30	180	10^{-4}	10^{-5}
GaAs	Dojo	90	70	40	8	8	31	104	130	130	20	150	10^{-4}	10^{-5}
Ge	Dojo	90	70	25	8	8	31	104	130	130	20	150	10^{-4}	10^{-5}
MgO	SG15	70	65	30	6	8	31	104	50	280	30	180	10^{-4}	10^{-5}
Si	SG15	20	19	15	8	8	31	104	50	280	40	200	10^{-4}	10^{-6}
BN [†]	SG15	60	30	10	1	4	21	67	50	50	2	100	10^{-4}	10^{-5}
Si [*]	SG15	16	15	12	8	8	201	768	800	100	351	35	10^{-10}	10^{-5}

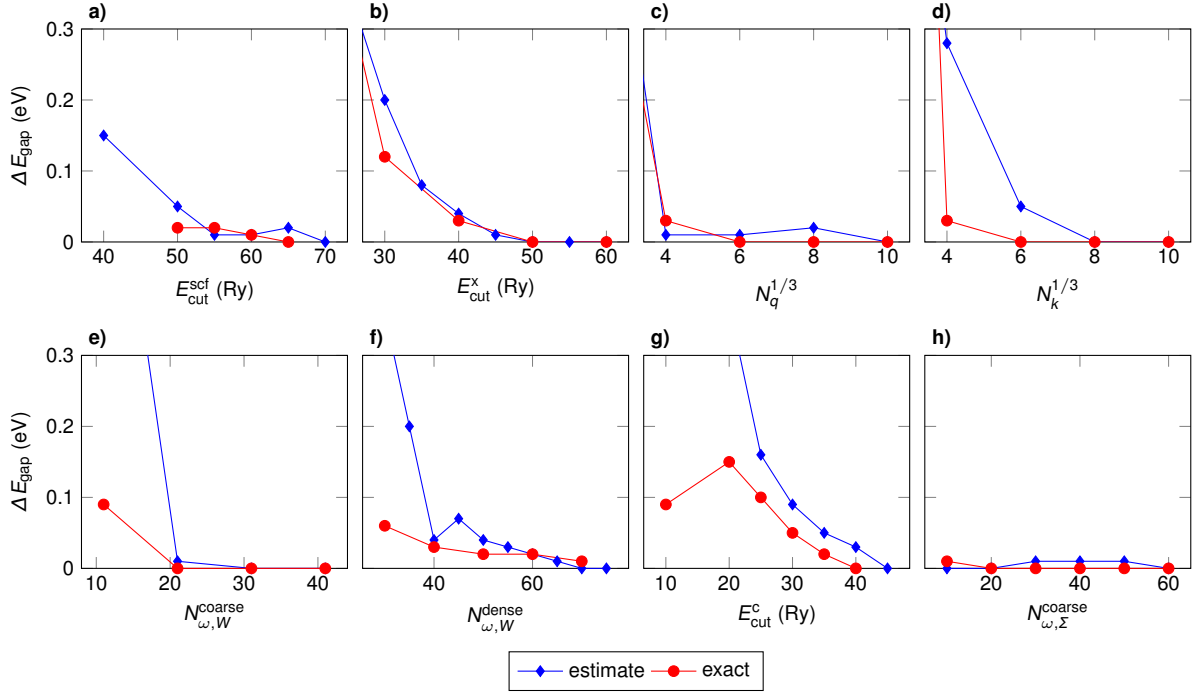


Figure 5: Convergence of the band gap of BN in the zincblende structure with respect to various convergence parameters in STERNHEIMERGW. The quantity ΔE_{gap} indicates the difference between the band gap with a given set of input parameters and the fully converged value $E_{\text{gap}} = 6.27$ eV. The blue line is obtained by varying one parameter at a time, while keeping the remaining parameters to loose values. The red line corresponds to calculations with the remaining parameters being set to stringent values. See section 3.2 for a detailed discussion of all parameters and Table 3 for the loose and stringent values used in the calculation.

STERNHEIMERGW v0.15. The STERNHEIMERGW calculations were converged using the algorithm described in Sec. 3.2 resulting in the parameters listed in Table 3. Overall, we find that our results agree well with the literature, within an error bar of 0.1 eV usually quoted in the literature for *GW* calculations.

3.2. Converging a *GW* calculation

Predictive *GW* calculations require the convergence of several numerical parameters. An efficient strategy is required to obtain these values at a reasonable computational cost. In order to tackle this multi-dimensional optimization, a possible strategy is to keep all convergence parameters at a loose setting, and only focus on the convergence behavior of a single parameter. To determine reasonable values for the loose setting it is a good strategy to focus on parts of the calculation that can be evaluated separately from the rest. First, one considers the exchange contribution to the *GW* self-energy, which is the most challenging quantity to converge in STERNHEIMERGW, but at the same time its calculation is significantly less demanding than the correlation part. The analysis of the exchange self-energy yields estimates for the wavefunction cutoff $E_{\text{cut}}^{\text{scf}}$ used in the DFT calculation (Fig. 5a), the exchange cutoff $E_{\text{cut}}^{\text{x}}$ (Fig. 5b), and the number $N_{\mathbf{q}}$ of points in the \mathbf{q} -point grid used

to evaluate the Brillouin-zone integrals (Fig. 5c). The wavefunction and the exchange cutoff are somewhat intertwined, and occasionally the former needs to be increased to allow for convergence of the latter. Secondly, we investigate the convergence of the head of the dielectric function ($\mathbf{q} = 0$ point) with respect to the number of \mathbf{k} points $N_{\mathbf{k}}$ (Fig. 5d) and the coarse frequency mesh $N_{\omega,W}^{\text{coarse}}$ used for the analytic continuation (Fig. 5e).

Guided by the initial studies of the exchange self-energy and the dielectric matrix, we construct the loose setting for the convergence study. In general, we will choose the smallest possible values in the smooth region of convergence. For the correlation, we need to set three further numerical parameters: For the dense frequency mesh $N_{\omega,W}^{\text{dense}}$ (Fig. 5f), we choose a mesh twice as dense as the coarse mesh; for the correlation cutoff $E_{\text{cut}}^{\text{c}}$ (Fig. 5g), we select typically a third of the value used for the exchange self-energy; and we use just two frequencies $N_{\omega,\Sigma}^{\text{coarse}} = 2$ (Fig. 5h) to perform the analytic continuation of the correlation self-energy from the imaginary to the real frequency axis.

With the constructed loose mesh, we then perform the convergence study individually increasing every single one of the parameters until the quasiparticle energies of interest are converged. The advantage of this strategy is that the computational cost of the complete conver-

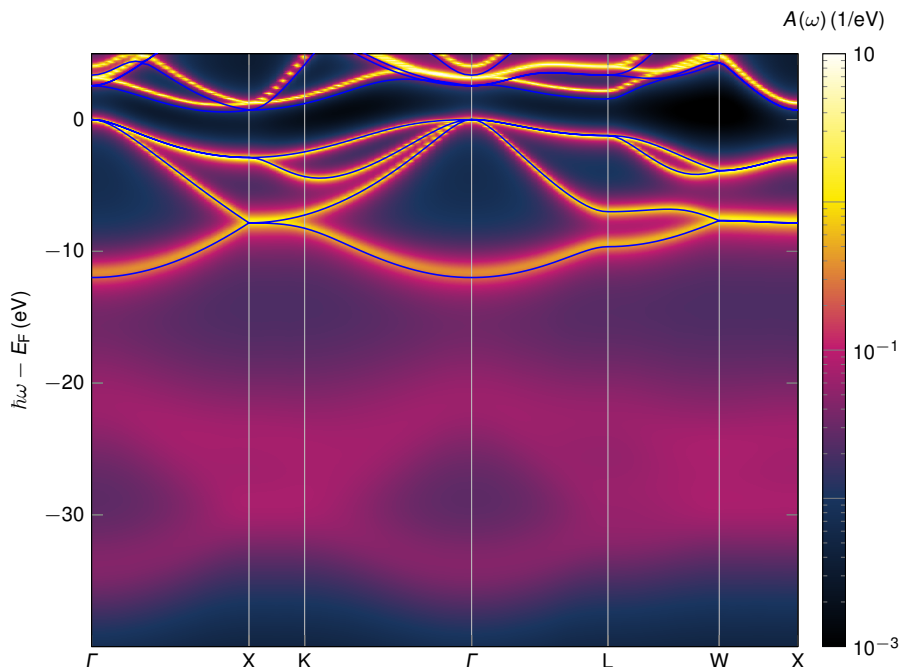


Figure 6: Spectral function of silicon along high-symmetry directions in the Brillouin zone. Results are obtained with full-frequency integration along the imaginary axis. For comparison the DFT bandstructure is shown as blue lines. Numerical parameters used for the calculations are listed in Table 3.

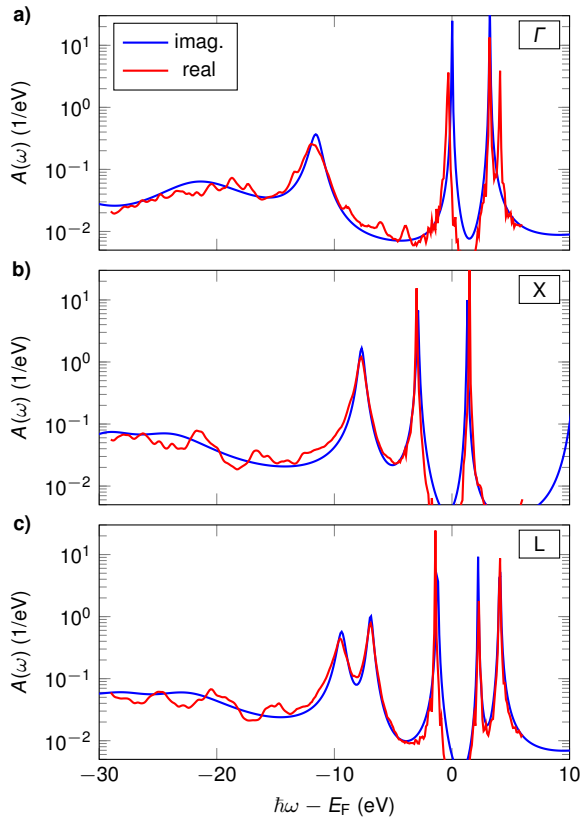


Figure 7: Comparison between spectral function $A(\omega)$ of silicon at **a)** the Γ point, **b)** the X point, and **c)** the L point when Σ^c is obtained by convolution along real (red) or imaginary (blue) frequency axis. The small shift in the valence band top is a consequence of the finite broadening $\eta = 0.15$ eV employed in the calculation of the Green's function. Numerical parameters used for the calculations are listed in Table 3.

gence study is significantly smaller than that of the subsequent GW calculation. In Fig. 5, we demonstrate that the estimate based on the loose setting provides a conservative estimate of the stringent parameters needed to obtain converged results.

3.3. Spectral function

One noteworthy feature of STERNHEIMERGW is the possibility of calculating the \mathbf{k} -resolved spectral function at any arbitrary point in the Brillouin zone. This feature allows us to compute GW band structures without the need for interpolation techniques. The frequency resolution provides insight into the electronic lifetimes, and can be directly compared to ARPES experiments. In Fig. 6, we show a representative calculation for silicon. We can see the quasiparticle bands and the weaker replica of the bands due to the plasmon satellite. We note that the energy and broadening of the plasmon

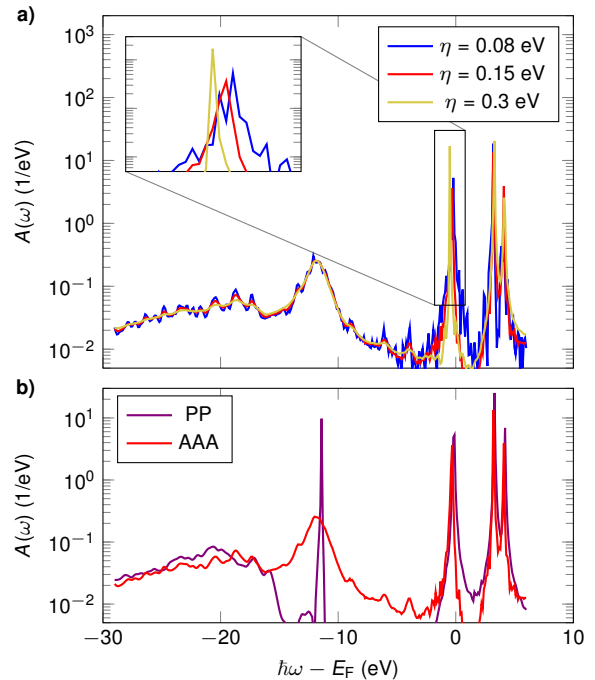


Figure 8: Impact of numerical technique on spectral function of silicon at Γ obtained by convolution along the real frequency axis. **a)** Increasing the smearing from $\eta = 0.08$ eV (blue) to 0.15 eV (red) or 0.3 eV (yellow) results in a decrease of the noise but also a shift of the valence band maximum to lower energies (see inset). **b)** Using the plasmon pole (PP) model (purple) instead of the AAA analytic continuation (blue) results in vanishing linewidths. We note that the vertical axes are on a logarithmic scale. Numerical parameters used for the calculations are listed in Table 3.

satellites are not accurately described in GW . An accurate description of these features requires the inclusion of higher order effects via the cumulant expansion.^{14,54,61–67}

3.4. Real frequency integration

As outlined in Sec. 2.4, STERNHEIMERGW provides the option to perform the frequency convolution along the real or the imaginary frequency axis. In Fig. 7, we demonstrate that these two implementations give nearly identical results for the spectral function at high-symmetry points of silicon. The main identifiable differences is a small shift of the valence band top to lower energies and an increased noise when using integration along the real axis. Both of these differences originate from the small parameter $\eta = 0.15$ eV that is used to shift the frequency slightly off the real axis. This shift is necessary in order to avoid the singularities on the real axis, so as to obtain numerically stable results. On the one hand, if η is decreased to 0.08 eV the resulting spectral function becomes very noisy (see Fig. 8a). On the

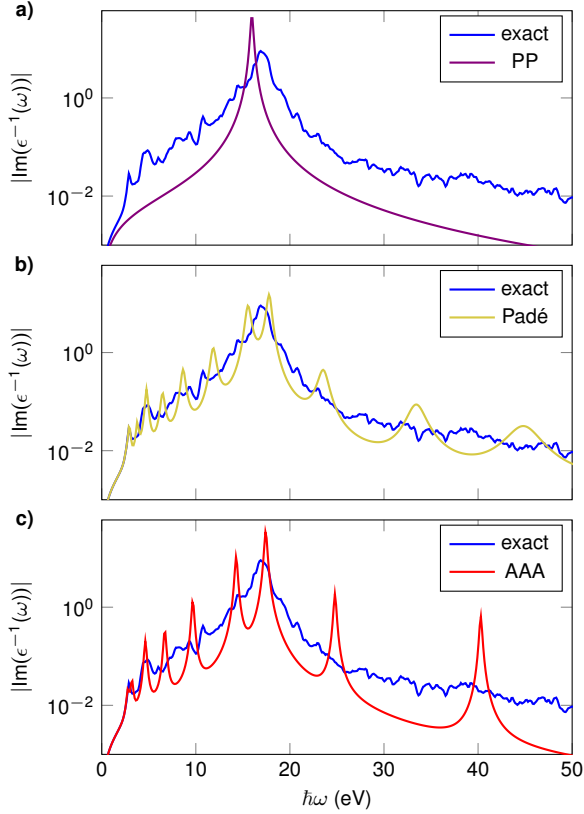


Figure 9: Inverse of the dielectric matrix of silicon at the Γ point obtained by solving the Sternheimer equation (6) along the real axis (blue) compared to **a**) plasmon pole model (purple), **b**) Padé expansion¹⁰⁷ (yellow), and **c**) AAA algorithm (red).¹⁰⁸ For the analytic continuation with either Padé or AAA, 201 frequencies along the imaginary axis were evaluated.

other hand, if η is increased to 0.3 eV, the energy of the quasiparticle becomes inaccurate (see inset of Fig. 8a).

In general, the integration along the imaginary axis with subsequent analytic continuation is one to two orders of magnitude cheaper because the Green's function and the screened Coulomb interaction have less structure there. As the results of both methods are very similar, we chose the integration along the imaginary axis as the default in STERNHEIMERGW, and we provide the integration along the real axis as an optional feature for validation.

In Fig. 8b, we show that obtaining accurate quasiparticle lifetimes requires going beyond the plasmon-pole approximation, because in this approximation there is only one sharp pole at the plasmon frequency (cf. Fig. 9a). In contrast, analytic continuation techniques can produce multiple poles and thereby capture the broadening of the quasiparticle spectra. In Fig. 9b,

we show that the Padé expansion¹⁰⁷ can reproduce the shape of the dielectric function more accurately than the plasmon-pole approximation, since it naturally incorporates multiple poles. However, this Padé algorithm is numerically not stable when using a large number of frequencies, therefore it cannot be used for the convolution along the real frequency axis. To address this issue, we employ the AAA analytic¹⁰⁸ continuation technique, whereby only significant frequencies are selected via a singular value decomposition. Subsequently, poles with weak residues are removed so that only the most important contributions remain. In Fig. 9c, we show that the AAA method reduces the number of poles compared to the Padé expansion while still reproducing the overall shape and magnitude of the dielectric matrix.

4. Conclusion

We presented the STERNHEIMERGW code, which calculates many-body *GW* self-energies, quasiparticle band structures, and spectral functions by solving linear-response Sternheimer equations. The linear response scheme allows us to calculate the *GW* self-energy at arbitrary \mathbf{k} points. This is particularly useful for computing band structures without resorting to interpolation techniques, and for comparison to ARPES experiments. STERNHEIMERGW goes beyond the plasmon-pole approximation by performing full-frequency integration along the real or the imaginary axis.

STERNHEIMERGW is aligned with the version 6.3 of Quantum Espresso. The dedicated website <http://www.sternheimergw.org> provides users with installation guidelines, tutorials, and a comprehensive documentation of all input variables. The code is efficiently parallelized and has been tested extensively on high-performance computing architectures. Updated versions of the code are distributed in the GitHub repository <https://github.com/QEF/SternheimerGW>.

Acknowledgments

The development of STERNHEIMERGW has received funding from the Leverhulme Trust (Grant RL-2012-001), the Graphene Flagship (Horizon 2020 Grant No. 785219 - GrapheneCore2), and the UK Engineering and Physical Sciences Research Council (Grant No. EP/M020517/1). Furthermore, the authors acknowledge the use of the University of Oxford Advanced Research Computing (ARC) facility (<http://dx.doi.org/10.5281/zenodo.22558>), the ARCHER UK National Supercomputing Service under

the T-Dops project, the Cambridge Service for Data Driven Discovery (CSD3) funded by EPSRC Tier-2 (Grant EP/P020259/1), the DECI resource Cartesius based in the Netherlands at SURFsara and Abel based in Oslo with support from the PRACE AISBL, and PRACE for awarding us access to MareNostrum at BSC-CNS, Spain.

References

- [1] B. Gumhalter, V. Kovač, F. Caruso, H. Lambert, F. Giustino, On the combined use of *GW* approximation and cumulant expansion in the calculations of quasiparticle spectra: The paradigm of Si valence bands, *Phys. Rev. B* 94 (2016) 035103. doi:10.1103/PhysRevB.94.035103.
- [2] C. Heil, M. Schlipf, F. Giustino, Quasiparticle *GW* band structures and Fermi surfaces of bulk and monolayer NbS₂, *Phys. Rev. B* 98 (2018) 075120. doi:10.1103/PhysRevB.98.075120.
- [3] P. Hohenberg, W. Kohn, Inhomogeneous electron gas, *Phys. Rev.* 136 (1964) B864–B871. doi:10.1103/PhysRev.136.B864.
- [4] W. Kohn, L. J. Sham, Self-consistent equations including exchange and correlation effects, *Phys. Rev.* 140 (1965) A1133–A1138. doi:10.1103/PhysRev.140.A1133.
- [5] R. O. Jones, Density functional theory: Its origins, rise to prominence, and future, *Rev. Mod. Phys.* 87 (2015) 897–923. doi:10.1103/RevModPhys.87.897.
- [6] J. P. Perdew, M. Levy, Physical content of the exact Kohn-Sham orbital energies: Band gaps and derivative discontinuities, *Phys. Rev. Lett.* 51 (1983) 1884–1887. doi:10.1103/PhysRevLett.51.1884.
- [7] L. J. Sham, M. Schlüter, Density-functional theory of the energy gap, *Phys. Rev. Lett.* 51 (1983) 1888–1891. doi:10.1103/PhysRevLett.51.1888.
- [8] L. Hedin, New method for calculating the one-particle Green's function with application to the electron-gas problem, *Phys. Rev.* 139 (1965) A796–A823. doi:10.1103/PhysRev.139.A796.
- [9] L. Hedin, S. O. Lundqvist, Effects of Electron-Electron and Electron-Phonon Interactions on the One-Electron States of Solids, Vol. 23 of Solid State Physics, Academic Press, 1969, pp. 1–181. doi:10.1016/S0081-1947(08)60615-3.
- [10] G. Strinati, H. J. Mattausch, W. Hanke, Dynamical correlation effects on the quasiparticle Bloch states of a covalent crystal, *Phys. Rev. Lett.* 45 (1980) 290–294. doi:10.1103/PhysRevLett.45.290.
- [11] G. Strinati, H. J. Mattausch, W. Hanke, Dynamical aspects of correlation corrections in a covalent crystal, *Phys. Rev. B* 25 (1982) 2867–2888. doi:10.1103/PhysRevB.25.2867.
- [12] M. S. Hybertsen, S. G. Louie, Electron correlation in semiconductors and insulators: Band gaps and quasiparticle energies, *Phys. Rev. B* 34 (1986) 5390–5413. doi:10.1103/PhysRevB.34.5390.
- [13] R. W. Godby, M. Schlüter, L. J. Sham, Accurate exchange-correlation potential for silicon and its discontinuity on addition of an electron, *Phys. Rev. Lett.* 56 (1986) 2415–2418. doi:10.1103/PhysRevLett.56.2415.
- [14] F. Aryasetiawan, O. Gunnarsson, The *GW* method, *Rep. Prog. Phys.* 61 (1998) 237. doi:10.1088/0034-4885/61/3/002.
- [15] W. G. Aulbur, M. Städele, A. Görling, Exact-exchange-based quasiparticle calculations, *Phys. Rev. B* 62 (2000) 7121–7132. doi:10.1103/PhysRevB.62.7121.
- [16] G. Onida, L. Reining, A. Rubio, Electronic excitations: density-functional versus many-body Green's-function approaches, *Rev. Mod. Phys.* 74 (2002) 601–659. doi:10.1103/RevModPhys.74.601.
- [17] M. Giantomassi, M. Stankovski, R. Shaltaf, M. Grüning, F. Bruneval, P. Rinke, G.-M. Rignanese, Electronic properties of interfaces and defects from many-body perturbation theory: Recent developments and applications, *Phys. Status Solidi B* 248 (2011) 275–289. doi:10.1002/pssb.201046094.
- [18] R. Shaltaf, G.-M. Rignanese, X. Gonze, F. Giustino, A. Pasquarello, Band offsets at the Si/SiO₂ interface from many-body perturbation theory, *Phys. Rev. Lett.* 100 (2008) 186401. doi:10.1103/PhysRevLett.100.186401.
- [19] P. Rinke, A. Janotti, M. Scheffler, C. G. Van de Walle, Defect formation energies without the band-gap problem: Combining density-functional theory and the *GW* approach for the silicon self-interstitial, *Phys. Rev. Lett.* 102 (2009) 026402. doi:10.1103/PhysRevLett.102.026402.
- [20] M. R. Filip, C. Verdi, F. Giustino, *GW* band structures and carrier effective masses of CH₃NH₃PbI₃ and hypothetical perovskites of the type APbI₃: A = NH₄, PH₄, AsH₄, and SbH₄, *J. Phys. Chem. C* 119 (2015) 25209–25219. doi:10.1021/acs.jpcc.5b07891.
- [21] C. Rostgaard, K. W. Jacobsen, K. S. Thygesen, Fully self-consistent *GW* calculations for molecules, *Phys. Rev. B* 81 (2010) 085103. doi:10.1103/PhysRevB.81.085103.
- [22] F. Caruso, P. Rinke, X. Ren, M. Scheffler, A. Rubio, Unified description of ground and excited states of finite systems: The self-consistent *GW* approach, *Phys. Rev. B* 86 (2012) 081102. doi:10.1103/PhysRevB.86.081102.
- [23] F. Caruso, P. Rinke, X. Ren, A. Rubio, M. Scheffler, Self-consistent *GW*: All-electron implementation with localized basis functions, *Phys. Rev. B* 88 (2013) 075105. doi:10.1103/PhysRevB.88.075105.
- [24] M. van Schilfgaarde, T. Kotani, S. Faleev, Quasiparticle self-consistent *GW* theory, *Phys. Rev. Lett.* 96 (2006) 226402. doi:10.1103/PhysRevLett.96.226402.
- [25] M. Gatti, F. Bruneval, V. Olevano, L. Reining, Understanding correlations in vanadium dioxide from first principles, *Phys. Rev. Lett.* 99 (2007) 266402. doi:10.1103/PhysRevLett.99.266402.
- [26] S. Ismail-Beigi, Correlation energy functional within the *GW*-RPA: Exact forms, approximate forms, and challenges, *Phys. Rev. B* 81 (2010) 195126. doi:10.1103/PhysRevB.81.195126.
- [27] B. I. Lundqvist, Single-particle spectrum of the degenerate electron gas, *Phys. kondens. Mater.* 6 (1967) 206–217. doi:10.1007/BF02422717.
- [28] B. I. Lundqvist, Single-particle spectrum of the degenerate electron gas, *Phys. kondens. Mater.* 7 (1968) 117–123. doi:10.1007/BF02422898.
- [29] D. C. Langreth, Singularities in the X-ray spectra of metals, *Phys. Rev. B* 1 (1970) 471–477. doi:10.1103/PhysRevB.1.471.
- [30] Y. Baer, G. Busch, X-ray photoemission from aluminum, *Phys. Rev. Lett.* 30 (1973) 280–282. doi:10.1103/PhysRevLett.30.280.
- [31] A. Bostwick, F. Speck, T. Seyller, K. Horn, M. Polini, R. Asgari, A. H. MacDonald, E. Rotenberg, Observation of plasmarons in quasi-freestanding doped graphene, *Science* 328 (2010) 999–1002. doi:10.1126/science.1186489.
- [32] M. Guzzo, G. Lani, F. Sottile, P. Romaniello, M. Gatti, J. J. Kas, J. J. Rehr, M. G. Silly, F. Sirotti, L. Reining, Valence electron photoemission spectrum of semiconductors: Ab initio description of multiple satellites, *Phys. Rev. Lett.* 107 (2011)

166401. doi:10.1103/PhysRevLett.107.166401.
- [33] M. Guzzo, J. Kas, F. Sottile, M. Silly, F. Sirotti, J. Rehr, L. Reining, Plasmon satellites in valence-band photoemission spectroscopy - ab initio study of the photon-energy dependence in semiconductors, *Eur. Phys. J. B* 85 (2012) 324. doi:10.1140/epjb/e2012-30267-y.
- [34] J. Lischner, D. Vigil-Fowler, S. G. Louie, Physical origin of satellites in photoemission of doped graphene: An ab initio GW plus cumulant study, *Phys. Rev. Lett.* 110 (2013) 146801. doi:10.1103/PhysRevLett.110.146801.
- [35] J. Lischner, D. Vigil-Fowler, S. G. Louie, Satellite structures in the spectral functions of the two-dimensional electron gas in semiconductor quantum wells: A GW plus cumulant study, *Phys. Rev. B* 89 (2014) 125430. doi:10.1103/PhysRevB.89.125430.
- [36] M. Guzzo, J. J. Kas, L. Sponza, C. Giorgetti, F. Sottile, D. Pierucci, M. G. Silly, F. Sirotti, J. J. Rehr, L. Reining, Multiple satellites in materials with complex plasmon spectra: From graphite to graphene, *Phys. Rev. B* 89 (2014) 085425. doi:10.1103/PhysRevB.89.085425.
- [37] J. J. Kas, J. J. Rehr, L. Reining, Cumulant expansion of the retarded one-electron Green function, *Phys. Rev. B* 90 (2014) 085112. doi:10.1103/PhysRevB.90.085112.
- [38] J. Lischner, G. K. Pálsson, D. Vigil-Fowler, S. Nemsak, J. Avila, M. C. Asensio, C. S. Fadley, S. G. Louie, Satellite band structure in silicon caused by electron-plasmon coupling, *Phys. Rev. B* 91 (2015) 205113. doi:10.1103/PhysRevB.91.205113.
- [39] F. Caruso, F. Giustino, Spectral fingerprints of electron-plasmon coupling, *Phys. Rev. B* 92 (2015) 045123. doi:10.1103/PhysRevB.92.045123.
- [40] F. Caruso, H. Lambert, F. Giustino, Band structures of plasmonic polarons, *Phys. Rev. Lett.* 114 (2015) 146404. doi:10.1103/PhysRevLett.114.146404.
- [41] F. Caruso, F. Giustino, The GW plus cumulant method and plasmonic polarons: application to the homogeneous electron gas, *Eur. Phys. J. B* 89 (2016) 238. doi:10.1140/epjb/e2016-70028-4.
- [42] F. Caruso, F. Giustino, Theory of electron-plasmon coupling in semiconductors, *Phys. Rev. B* 94 (2016) 115208. doi:10.1103/PhysRevB.94.115208.
- [43] F. Caruso, C. Verdi, S. Poncé, F. Giustino, Electron-plasmon and electron-phonon satellites in the angle-resolved photoelectron spectra of *n*-doped anatase TiO₂, *Phys. Rev. B* 97 (2018) 165113. doi:10.1103/PhysRevB.97.165113.
- [44] H. Fröhlich, Electrons in lattice fields, *Adv. Phys.* 3 (11) (1954) 325–361. doi:10.1080/00018735400101213.
- [45] Y. J. Chang, A. Bostwick, Y. S. Kim, K. Horn, E. Rotenberg, Structure and correlation effects in semiconducting SrTiO₃, *Phys. Rev. B* 81 (2010) 235109. doi:10.1103/PhysRevB.81.235109.
- [46] S. Moser, L. Moreschini, J. Jaćimović, O. S. Barišić, H. Berger, A. Magrez, Y. J. Chang, K. S. Kim, A. Bostwick, E. Rotenberg, L. Forró, M. Grioni, Tunable polaronic conduction in anatase TiO₂, *Phys. Rev. Lett.* 110 (2013) 196403. doi:10.1103/PhysRevLett.110.196403.
- [47] P. D. C. King, S. McKeown Walker, A. Tamai, A. de la Torre, T. Eknapakul, P. Buaphet, S.-K. Mo, W. Meevasana, M. S. Bahramy, F. Baumberger, Quasiparticle dynamics and spin-orbital texture of the SrTiO₃ two-dimensional electron gas, *Nat. Commun.* 5 (2014) 3414. doi:10.1038/ncomms4414.
- [48] S. M. Story, J. J. Kas, F. D. Vila, M. J. Verstraete, J. J. Rehr, Cumulant expansion for phonon contributions to the electron spectral function, *Phys. Rev. B* 90 (2014) 195135. doi:10.1103/PhysRevB.90.195135.
- [49] G. Antonius, S. Poncé, E. Lantagne-Hurtubise, G. Auclair, X. Gonze, M. Côté, Dynamical and anharmonic effects on the electron-phonon coupling and the zero-point renormalization of the electronic structure, *Phys. Rev. B* 92 (2015) 085137. doi:10.1103/PhysRevB.92.085137.
- [50] C. Chen, J. Avila, E. Frantzeskakis, A. Levy, M. C. Asensio, Observation of a two-dimensional liquid of Fröhlich polarons at the bare SrTiO₃ surface, *Nat. Commun.* 6 (2015) 8585. doi:10.1038/ncomms9585.
- [51] Z. Wang, S. McKeown Walker, A. Tamai, Y. Wang, Z. Ristic, F. Y. Bruno, A. de la Torre, S. Riccò, N. C. Plumb, M. Shi, P. Hlawenka, J. Sánchez-Barriga, A. Varykhalov, T. K. Kim, M. Hoesch, P. D. C. King, W. Meevasana, U. Diebold, J. Mesot, B. Moritz, T. P. Devereaux, M. Radovic, F. Baumberger, Tailoring the nature and strength of electron-phonon interactions in the SrTiO₃(001) 2D electron liquid, *Nat. Mater.* 15 (2016) 835. doi:10.1038/nmat4623.
- [52] C. Cancellieri, A. S. Mishchenko, U. Aschauer, A. Filippetti, C. Faber, O. S. Barišić, V. A. Rogalev, T. Schmitt, N. Nagaosa, V. N. Strocov, Polaronic metal state at the LaAlO₃/SrTiO₃ interface, *Nat. Commun.* 7 (2016) 10386. doi:10.1038/ncomms10386.
- [53] R. Yukawa, K. Ozawa, S. Yamamoto, H. Iwasawa, K. Shimada, E. F. Schwier, K. Yoshimatsu, H. Kumigashira, H. Namatame, M. Taniguchi, I. Matsuda, Phonon-dressed two-dimensional carriers on the ZnO surface, *Phys. Rev. B* 94 (2016) 165313. doi:10.1103/PhysRevB.94.165313.
- [54] C. Verdi, F. Caruso, F. Giustino, Origin of the crossover from polarons to Fermi liquids in transition metal oxides, *Nat. Commun.* 8 (2017) 15769. doi:10.1038/ncomms15769.
- [55] J. P. Nery, P. B. Allen, G. Antonius, L. Reining, A. Miglio, X. Gonze, Quasiparticles and phonon satellites in spectral functions of semiconductors and insulators: Cumulants applied to the full first-principles theory and the Fröhlich polaron, *Phys. Rev. B* 97 (2018) 115145. doi:10.1103/PhysRevB.97.115145.
- [56] M. Settnes, J. R. M. Saavedra, K. S. Thygesen, A.-P. Jauho, F. J. Garca de Abajo, N. A. Mortensen, Strong plasmon-phonon splitting and hybridization in 2D materials revealed through a self-energy approach, *ACS Photonics* 4 (11) (2017) 2908–2915. doi:10.1021/acsp Photonics.7b00928.
- [57] J. M. Riley, F. Caruso, C. Verdi, L. B. Duffy, M. D. Watson, L. Bawden, K. Volckaert, G. van der Laan, T. Hesjedal, M. Hoesch, F. Giustino, P. D. C. King, Crossover from lattice to plasmonic polarons of a spin-polarised electron gas in ferromagnetic EuO, *Nat. Commun.* 9 (1) (2018) 2305. doi:10.1038/s41467-018-04749-w.
- [58] A. S. Kheifets, V. A. Sashin, M. Vos, E. Weigold, F. Aryasetiawan, Spectral properties of quasiparticles in silicon: A test of many-body theory, *Phys. Rev. B* 68 (2003) 233205. doi:10.1103/PhysRevB.68.233205.
- [59] B. Holm, U. von Barth, Fully self-consistent GW self-energy of the electron gas, *Phys. Rev. B* 57 (1998) 2108–2117. doi:10.1103/PhysRevB.57.2108.
- [60] A. Kutepov, K. Haule, S. Y. Savrasov, G. Kotliar, Electronic structure of Pu and Am metals by self-consistent relativistic GW method, *Phys. Rev. B* 85 (2012) 155129. doi:10.1103/PhysRevB.85.155129.
- [61] F. Aryasetiawan, L. Hedin, K. Karlsson, Multiple plasmon satellites in Na and Al spectral functions from ab initio cumulant expansion, *Phys. Rev. Lett.* 77 (1996) 2268–2271. doi:10.1103/PhysRevLett.77.2268.
- [62] B. Holm, F. Aryasetiawan, Self-consistent cumulant expansion for the electron gas, *Phys. Rev. B* 56 (1997) 12825–12831. doi:10.1103/PhysRevB.56.12825.

- [63] L. Hedin, On correlation effects in electron spectroscopies and the GW approximation, *J. Phys.: Condens. Matter* 11 (42) (1999) R489. doi:10.1088/0953-8984/11/42/201.
- [64] B. Gumhalter, Ultrafast dynamics and decoherence of quasiparticles in surface bands: Development of the formalism, *Phys. Rev. B* 72 (2005) 165406. doi:10.1103/PhysRevB.72.165406.
- [65] B. Gumhalter, Stages of hot electron dynamics in multiexcitation processes at surfaces: General properties and benchmark examples, *Prog. Surf. Sci.* 87 (2012) 163 – 188. doi:https://doi.org/10.1016/j.progsurf.2012.05.004.
- [66] J. S. Zhou, J. J. Kas, L. Sponza, I. Reshetnyak, M. Guzzo, C. Giorgetti, M. Gatti, F. Sottile, J. J. Rehr, L. Reining, Dynamical effects in electron spectroscopy, *J. Chem. Phys.* 143 (2015) 184109. doi:10.1063/1.4934965.
- [67] F. Caruso, C. Verdi, F. Giustino, Many-Body Calculations of Plasmon and Phonon Satellites in Angle-Resolved Photoelectron Spectra Using the Cumulant Expansion Approach, Springer International Publishing, Cham, 2018, pp. 1–25. doi:10.1007/978-3-319-42913-7_2-1.
- [68] R. W. Godby, R. J. Needs, Metal-insulator transition in Kohn-Sham theory and quasiparticle theory, *Phys. Rev. Lett.* 62 (1989) 1169–1172. doi:10.1103/PhysRevLett.62.1169.
- [69] G. E. Engel, B. Farid, Generalized plasmon-pole model and plasmon band structures of crystals, *Phys. Rev. B* 47 (1993) 15931–15934. doi:10.1103/PhysRevB.47.15931.
- [70] R. Daling, W. van Haeringen, B. Farid, Plasmon dispersion in silicon obtained by analytic continuation of the random-phase-approximation dielectric matrix, *Phys. Rev. B* 44 (1991) 2952–2960. doi:10.1103/PhysRevB.44.2952.
- [71] H. N. Rojas, R. W. Godby, R. J. Needs, Space-time method for ab initio calculations of self-energies and dielectric response functions of solids, *Phys. Rev. Lett.* 74 (1995) 1827–1830. doi:10.1103/PhysRevLett.74.1827.
- [72] Y.-G. Jin, K. J. Chang, Dynamic response function and energy-loss spectrum for Li using an N -point Padé approximant, *Phys. Rev. B* 59 (1999) 14841–14844. doi:10.1103/PhysRevB.59.14841.
- [73] R. W. Godby, M. Schlüter, L. J. Sham, Self-energy operators and exchange-correlation potentials in semiconductors, *Phys. Rev. B* 37 (1988) 10159–10175. doi:10.1103/PhysRevB.37.10159.
- [74] T. Kotani, M. van Schilfhaarde, All-electron GW approximation with the mixed basis expansion based on the full-potential LMTO method, *Solid State Commun.* 121 (9) (2002) 461 – 465. doi:https://doi.org/10.1016/S0038-1098(02)00028-5.
- [75] S. Lebègue, B. Arnaud, M. Alouani, P. E. Blochl, Implementation of an all-electron GW approximation based on the projector augmented wave method without plasmon pole approximation: Application to Si, SiC, AlAs, InAs, NaH, and KH, *Phys. Rev. B* 67 (2003) 155208. doi:10.1103/PhysRevB.67.155208.
- [76] C. D. Spataru, M. A. Cazalilla, A. Rubio, L. X. Benedict, P. M. Echenique, S. G. Louie, Anomalous quasiparticle lifetime in graphite: Band structure effects, *Phys. Rev. Lett.* 87 (2001) 246405. doi:10.1103/PhysRevLett.87.246405.
- [77] C.-H. Park, F. Giustino, C. D. Spataru, M. L. Cohen, S. G. Louie, Angle-resolved photoemission spectra of graphene from first-principles calculations, *Nano Lett.* 9 (2009) 4234–4239. doi:10.1021/nl902448v.
- [78] B.-C. Shih, Y. Xue, P. Zhang, M. L. Cohen, S. G. Louie, Quasiparticle band gap of ZnO: High accuracy from the conventional G^0W^0 approach, *Phys. Rev. Lett.* 105 (2010) 146401. doi:10.1103/PhysRevLett.105.146401.
- [79] C. Friedrich, M. C. Müller, S. Blügel, Band convergence and linearization error correction of all-electron GW calculations: The extreme case of zinc oxide, *Phys. Rev. B* 83 (2011) 081101. doi:10.1103/PhysRevB.83.081101.
- [80] M. Stankovski, G. Antonius, D. Waroquiers, A. Miglio, H. Dixit, K. Sankaran, M. Giantomassi, X. Gonze, M. Côté, G.-M. Rignanese, G^0W^0 band gap of ZnO: Effects of plasmon-pole models, *Phys. Rev. B* 84 (2011) 241201. doi:10.1103/PhysRevB.84.241201.
- [81] M. J. van Setten, M. Giantomassi, X. Gonze, G.-M. Rignanese, G. Hautier, Automation methodologies and large-scale validation for GW : Towards high-throughput GW calculations, *Phys. Rev. B* 96 (2017) 155207. doi:10.1103/PhysRevB.96.155207.
- [82] F. Bruneval, X. Gonze, Accurate GW self-energies in a plane-wave basis using only a few empty states: Towards large systems, *Phys. Rev. B* 78 (2008) 085125. doi:10.1103/PhysRevB.78.085125.
- [83] W. Kang, M. S. Hybertsen, Enhanced static approximation to the electron self-energy operator for efficient calculation of quasiparticle energies, *Phys. Rev. B* 82 (2010) 195108. doi:10.1103/PhysRevB.82.195108.
- [84] J. A. Berger, L. Reining, F. Sottile, Ab initio calculations of electronic excitations: Collapsing spectral sums, *Phys. Rev. B* 82 (2010) 041103. doi:10.1103/PhysRevB.82.041103.
- [85] J. A. Berger, L. Reining, F. Sottile, Efficient GW calculations for SnO_2 , ZnO, and rubrene: The effective-energy technique, *Phys. Rev. B* 85 (2012) 085126. doi:10.1103/PhysRevB.85.085126.
- [86] J. Deslippe, G. Samsonidze, M. Jain, M. L. Cohen, S. G. Louie, Coulomb-hole summations and energies for GW calculations with limited number of empty orbitals: A modified static remainder approach, *Phys. Rev. B* 87 (2013) 165124. doi:10.1103/PhysRevB.87.165124.
- [87] W. Gao, W. Xia, X. Gao, P. Zhang, Speeding up GW calculations to meet the challenge of large scale quasiparticle predictions, *Sci. Rep.* 6 (2016) 36849. doi:10.1038/srep36849.
- [88] S. Baroni, P. Giannozzi, A. Testa, Green’s-function approach to linear response in solids, *Phys. Rev. Lett.* 58 (1987) 1861–1864. doi:10.1103/PhysRevLett.58.1861.
- [89] S. Baroni, S. de Gironcoli, A. Dal Corso, P. Giannozzi, Phonons and related crystal properties from density-functional perturbation theory, *Rev. Mod. Phys.* 73 (2001) 515–562. doi:10.1103/RevModPhys.73.515.
- [90] L. Reining, G. Onida, R. W. Godby, Elimination of unoccupied-state summations in ab initio self-energy calculations for large supercells, *Phys. Rev. B* 56 (1997) R4301–R4304. doi:10.1103/PhysRevB.56.R4301.
- [91] H. F. Wilson, F. Gygi, G. Galli, Efficient iterative method for calculations of dielectric matrices, *Phys. Rev. B* 78 (2008) 113303. doi:10.1103/PhysRevB.78.113303.
- [92] H. F. Wilson, D. Lu, F. Gygi, G. Galli, Iterative calculations of dielectric eigenvalue spectra, *Phys. Rev. B* 79 (2009) 245106. doi:10.1103/PhysRevB.79.245106.
- [93] T. A. Pham, H.-V. Nguyen, D. Rocca, G. Galli, GW calculations using the spectral decomposition of the dielectric matrix: Verification, validation, and comparison of methods, *Phys. Rev. B* 87 (2013) 155148. doi:10.1103/PhysRevB.87.155148.
- [94] P. Umari, G. Stenuit, S. Baroni, Optimal representation of the polarization propagator for large-scale GW calculations, *Phys. Rev. B* 79 (2009) 201104. doi:10.1103/PhysRevB.79.201104.
- [95] P. Umari, G. Stenuit, S. Baroni, GW quasiparticle spectra from occupied states only, *Phys. Rev. B* 81 (2010) 115104. doi:

- 10.1103/PhysRevB.81.115104.
- [96] F. Giustino, M. L. Cohen, S. G. Louie, *GW* method with the self-consistent Sternheimer equation, *Phys. Rev. B* 81 (2010) 115105. doi:10.1103/PhysRevB.81.115105.
- [97] M. Govoni, G. Galli, Large scale *GW* calculations, *J. Chem. Theory Comput.* 11 (2015) 2680–2696. doi:10.1021/ct500958p.
- [98] H. Lambert, F. Giustino, *Ab initio* Sternheimer-*GW* method for quasiparticle calculations using plane waves, *Phys. Rev. B* 88 (2013) 075117. doi:10.1103/PhysRevB.88.075117.
- [99] C. Heil, S. Poncé, H. Lambert, M. Schlipf, E. R. Margine, F. Giustino, Origin of superconductivity and latent charge density wave in NbS₂, *Phys. Rev. Lett.* 119 (2017) 087003. doi:10.1103/PhysRevLett.119.087003.
- [100] A. Frommer, BiCGStab(l) for families of shifted linear systems, *Computing* 70 (2003) 87–109. doi:10.1007/s00607-003-1472-6.
- [101] M. S. Hybertsen, S. G. Louie, *Ab initio* static dielectric matrices from the density-functional approach. I. formulation and application to semiconductors and insulators, *Phys. Rev. B* 35 (1987) 5585–5601. doi:10.1103/PhysRevB.35.5585.
- [102] One can correct the head of the dielectric matrix for evaluating it at a finite q .¹⁰³ However we do not include this correction, because it poses numerical difficulties and vanishes with increasing size of the q -point mesh. This approximation reduces the band gap slightly, for example from 7.19 eV to 7.13 eV in MgO.
- [103] L. Martin-Samos, G. Bussi, Sax: An open source package for electronic-structure and optical-properties calculations in the *gw* approximation, *Comput. Phys. Commun.* 180 (2009) 1416. doi:https://doi.org/10.1016/j.cpc.2009.02.005.
- [104] S. Ismail-Beigi, Truncation of periodic image interactions for confined systems, *Phys. Rev. B* 73 (2006) 233103. doi:10.1103/PhysRevB.73.233103.
- [105] C. A. Rozzi, D. Varsano, A. Marini, E. K. U. Gross, A. Rubio, Exact Coulomb cutoff technique for supercell calculations, *Phys. Rev. B* 73 (2006) 205119. doi:10.1103/PhysRevB.73.205119.
- [106] R. Sundararaman, T. A. Arias, Regularization of the Coulomb singularity in exact exchange by Wigner-Seitz truncated interactions: Towards chemical accuracy in nontrivial systems, *Phys. Rev. B* 87 (2013) 165122. doi:10.1103/PhysRevB.87.165122.
- [107] H. Vidberg, J. Serene, Solving the Eliashberg equations by means of *N*-point Padé approximants, *J. Low Temp. Phys.* 29 (1977) 179–192. doi:10.1007/BF00655090.
- [108] Y. Nakatsukasa, O. Sète, L. Trefethen, The AAA algorithm for rational approximation, *SIAM J. Sci. Comput.* 40 (2018) A1494–A1522. doi:10.1137/16M1106122.
- [109] P. Giannozzi, S. Baroni, N. Bonini, M. Calandra, R. Car, C. Cavazzoni, D. Ceresoli, G. L. Chiarotti, M. Cococcioni, I. Dabo, A. Dal Corso, S. de Gironcoli, S. Fabris, G. Fratesi, R. Gebauer, U. Gerstmann, C. Gougoussis, A. Kokalj, M. Lazzeri, L. Martin-Samos, N. Marzari, F. Mauri, R. Mazzarello, S. Paolini, A. Pasquarello, L. Paulatto, C. Sbraccia, S. Scandolo, G. Sclauzero, A. P. Seitsonen, A. Smogunov, P. Umari, R. M. Wentzcovitch, Quantum ESPRESSO: a modular and open-source software project for quantum simulations of materials, *J. Phys.: Condens. Matter* 21 (2009) 395502. doi:10.1088/0953-8984/21/39/395502. URL <http://www.quantum-espresso.org>
- [110] P. Giannozzi, O. Andreussi, T. Brumme, O. Bunau, M. B. Nardelli, M. Calandra, R. Car, C. Cavazzoni, D. Ceresoli, M. Cococcioni, N. Colonna, I. Carnimeo, A. D. Corso, S. de Gironcoli, P. Delugas, R. DiStasio, A. Ferretti, A. Floris, G. Fratesi, G. Fugallo, R. Gebauer, U. Gerstmann, F. Giustino, T. Gorni, J. Jia, M. Kawamura, H.-Y. Ko, A. Kokalj, E. Küçükbenli, M. Lazzeri, M. Marsili, N. Marzari, F. Mauri, N. L. Nguyen, H.-V. Nguyen, A. O. de-la Roza, L. Paulatto, S. Poncé, D. Rocca, R. Sabatini, B. Santra, M. Schlipf, A. P. Seitsonen, A. Smogunov, I. Timrov, T. Thonhauser, P. Umari, N. Vast, X. Wu, S. Baroni, Advanced capabilities for materials modelling with Quantum ESPRESSO, *J. Phys.: Condens. Matter* 29 (2017) 465901. doi:10.1088/1361-648X/aa8f79.
- [111] J. Spencer, testcode, <https://github.com/jsspencer/testcode> (2017).
- [112] Quantum ESPRESSO test farm with 3 configurations, <http://130.186.13.198:8010/>.
- [113] M. Rilee, T. Clune, Towards test driven development for computational science with pFUnit, in: Proceedings of the 2nd International Workshop on Software Engineering for High Performance Computing in Computational Science and Engineering, SE-HPCCSE '14, IEEE Press, Piscataway, NJ, USA, 2014, pp. 20–27. doi:10.1109/SE-HPCCSE.2014.5.
- [114] M. Shishkin, G. Kresse, Self-consistent *GW* calculations for semiconductors and insulators, *Phys. Rev. B* 75 (2007) 235102. doi:10.1103/PhysRevB.75.235102.
- [115] C. Friedrich, M. Betzinger, M. Schlipf, S. Blügel, A. Schindlmayr, Hybrid functionals and *GW* approximation in the FLAPW method, *J. Phys.: Condens. Matter* 24 (2012) 293201. doi:10.1088/0953-8984/24/29/293201.
- [116] W. Chen, A. Pasquarello, Band-edge positions in *GW*: Effects of starting point and self-consistency, *Phys. Rev. B* 90 (2014) 165133. doi:10.1103/PhysRevB.90.165133.
- [117] W. Chen, A. Pasquarello, Accurate band gaps of extended systems via efficient vertex corrections in *GW*, *Phys. Rev. B* 92 (2015) 041115. doi:10.1103/PhysRevB.92.041115.
- [118] M. Schlipf, F. Gygi, Optimization algorithm for the generation of ONCV pseudopotentials, *Comput. Phys. Comm.* 196 (2015) 36. doi:http://dx.doi.org/10.1016/j.cpc.2015.05.011.
- [119] M. van Setten, M. Giantomassi, E. Bousquet, M. Verstraete, D. Hamann, X. Gonze, G.-M. Rignanese, The PseudoDojo: Training and grading a 85 element optimized norm-conserving pseudopotential table, *Comput. Phys. Commun.* 226 (2018) 39. doi:https://doi.org/10.1016/j.cpc.2018.01.012.
- [120] R. Colella, B. Reinhart, E. Alp, E. E. Haller, Thermal Expansion of Germanium Isotopes at Low Temperature, *ArXiv e-prints* (2009) 0910.1569arXiv:0910.1569.
- [121] J. P. Perdew, K. Burke, M. Ernzerhof, Generalized gradient approximation made simple, *Phys. Rev. Lett.* 77 (1996) 3865–3868. doi:10.1103/PhysRevLett.77.3865.
- [122] K. Lejaeghere, G. Bihlmayer, T. Björkman, P. Blaha, S. Blügel, V. Blum, D. Caliste, I. E. Castelli, S. J. Clark, A. Dal Corso, S. de Gironcoli, T. Deutsch, J. K. Dewhurst, I. Di Marco, C. Draxl, M. Dułak, O. Eriksson, J. A. Flores-Livas, K. F. Garrity, L. Genovese, P. Giannozzi, M. Giantomassi, S. Goedecker, X. Gonze, O. Grånäs, E. K. U. Gross, A. Gulans, F. Gygi, D. R. Hamann, P. J. Hasnip, N. A. W. Holzwarth, D. Iuşan, D. B. Jochym, F. Jollet, D. Jones, G. Kresse, K. Koepf, E. Küçükbenli, Y. O. Kvashnin, I. L. M. Locht, S. Lubeck, M. Marsman, N. Marzari, U. Nitzsche, L. Nordström, T. Ozaki, L. Paulatto, C. J. Pickard, W. Poelmans, M. I. J. Probert, K. Refson, M. Richter, G.-M. Rignanese, S. Saha, M. Scheffler, M. Schlipf, K. Schwarz, S. Sharma, F. Tavazza, P. Thunström, A. Tkatchenko, M. Torrent, D. Vanderbilt, M. J. van Setten, V. Van Speybroeck, J. M. Wills, J. R. Yates, G.-X. Zhang, S. Cottenier, Reproducibility in density functional theory calculations of solids, *Science* 351 (2016) aad3000. doi:10.1126/science.aad3000.

- [123] D. R. Hamann, Optimized norm-conserving Vanderbilt pseudopotentials, *Phys. Rev. B* 88 (2013) 085117. doi:10.1103/PhysRevB.88.085117.